Particle Flow during Sawtooth Reconnection: Numerical Simulations of Experimental Observations*)

Timothée NICOLAS, Roland SABOT, Xavier GARBET, Hinrich LÜTJENS[1)], Jean-François LUCIANI[1)], Antoine SIRINELLI[2)], Joan DECKER, Antoine MERLE and JET-EFDA Contributors[3)]

CEA, IRFM, St-Paul-Lèz-Durance, France
[1)]*Centre de Physique Théorique, École Polytechnique, Palaiseau, France*
[2)]*Euratom/CCFE, Culham Science Centre, Abingdon, Oxon, OX14 3DB, UK*
[3)]*JET-EFDA, Culham Science Centre, Abingdon, Oxon, OX14 3DB, UK*

(Received 5 December 2012 / Accepted 2 August 2013)

The core plasma density in ohmic, sawtoothing regime in Tore Supra and JET tokamaks measured by fast-sweeping reflectometry develops a central peak. This peak is surrounded by a density plateau, which extends up to the $q = 1$ reconnection surface. Such mexican hat like profiles differ from the smooth dome of the temperature profile. Detailed tomographic reconstructions of the density in the poloidal plane show the development of crescent and ring structures during the sawtooth cycle. 3D full MHD nonlinear simulations with the XTOR-2F code recover these structures and show that they can be explained by the MHD activity related to the sawtooth instability. They show also that the electron density evolution is dominated by the perpendicular MHD flows, while the temperature, obtained with ECE measurements is dominated by parallel diffusion.

Keywords: reflectometry, MHD simulation, sawtooth instability and kink mode, Tore Supra, JET

DOI: 10.1585/pfr.8.2402131

1. Introduction

Sawteeth are relaxation oscillations affecting the core density and temperature of the plasma, triggered by an $m/n = 1/1$ MHD instabiliy, where m and n are the poloidal and toroidal wave numbers. Since the fusion power P_{fus} is proportional to the square of the pressure $p = nT$, this issue is of central importance, both temperature and density being reduced by typically 10% [1]. However, while the temperature relaxation, diffusion and heat pulse propagation have been extensively analyzed, density evolution has not been thoroughly studied. Complete homogenization is usually assumed after the sawtooth crash with a flat density profile inside the $q = 1$ surface [2]. Sawtooth relaxations are also crucial for core impurity transport. For future tokamaks, there must be an efficient way of evacuating the Helium produced by fusion reactions in the core, as well as flushing out high-Z impurities like Tungsten. It was lately reported in JET with the ITER-like wall that Tungsten ablated from the divertor was liable to accumulate in the core in H-mode, leading to back transitions to L-mode [3], and sometimes to the collapse of the discharge.

In this contribution, we present new elements based on recent experimental and numerical results regarding the density evolution linked with MHD activity in sawtooth regime. Experimental results are obtained using fast-sweeping X-mode reflectometry on Tore Supra [4, 5] and JET tokamaks while numerical simulations are carried out with the 3D full MHD nonlinear XTOR-2F [6] code.

On both devices, in ohmic regime, the density exhibits very characteristic structures, with amplitudes between 1% and 10% of the central density. The structures can be recovered with XTOR-2F, which has been used to understand the mechanism of their formation. In the experiment, a significant fraction (typically 30%), of the core density is not evacuated through the $q = 1$ surface, but is reorganized in the form of a crescent-shaped structure, visible both in the experiment and the simulation. The experimental results are described in section 2. In section 3, the numerical methods are presented. The numerical results are presented and compared with the experiment in section 4.

2. Experimental Results

Reflectometry is based on radar principle, measuring the phase of a microwave reflected from a plasma cutoff layer as a function of the probing frequency [7]. Depending on the polarization, the cutoff layer position depends on the local plasma density (Ordinary mode) and local magnetic intensity (eXtraordinary mode). The measured phase during a frequency sweep can be inverted to recover the cutoff layer positions and hence the density profile. Fast frequency sweeping increases the profile reliability like a fast shutter photography, the density profile is frozen dur-

author's e-mail: timothee.nicolas@cea.fr
*) This article is based on the presentation at the 22nd International Toki Conference (ITC22).

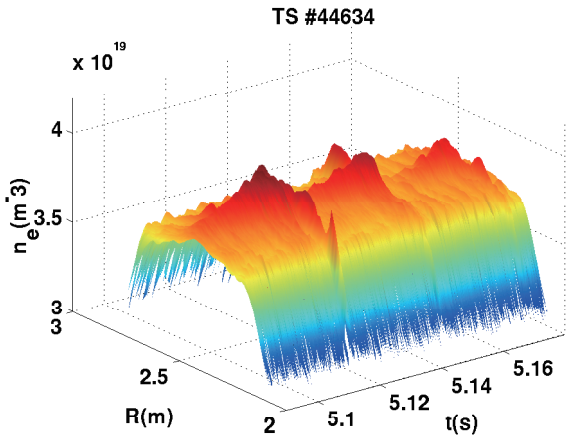

Fig. 1 Time trace of a series of sawtooth crashes, on the Tore Supra tokamak, pulse #44634.

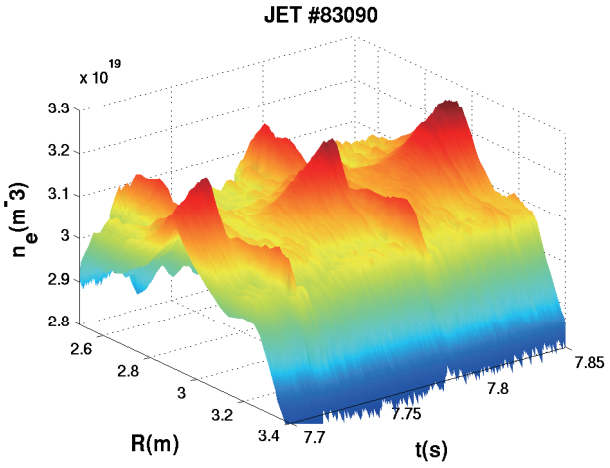

Fig. 2 Time trace of a series of sawtooth crashes, on the JET tokamak, pulse #83090.

ing the measurement [8].

2.1 Tore Supra results

On Tore Supra, the density profile is reconstructed using three X-mode reflectometers covering the band 50 to 155 GHz [9]. The D-band reflectometer (100 - 155 GHz) measures the density profile from the gradient zone on the outer side to the inner side in 30 to 70 µs [4]. The dwelt time between two consecutive sweeps can be as short as 5 µs and up to 10000 profiles can be stored in a shot. As the lowest frequency (100 GHz) is always inside the plasma, the profile inversion requires an initialization on an edge density profile measured either by the edge reflectometer or the interferometry diagnostic [10]. Uncertainty on calibration, equilibrium, magnetic field results on a global uncertainty of the radial position of 1 to 2 cm. However, the relative radial uncertainty from profile to profile is almost one order of magnitude lower. The density profile inside the $q = 1$ surface in ohmic shots at moderate density exhibits a peak inside the $q = 1$ surface surrounded by a density plateau as shown on Fig. 1. In this example, the plasma parameters are as follows : magnetic field on axis $B_0 = 3.8$ T, minor radius $a = 0.72$ m, major radius $R_0 = 2.4$ m, core density $n_0 = 3.8 \times 10^{19}$ m^{-3}, core electron temperature $T_{e0} = 2.4$ keV, poloidal beta (for a parabolic pressure profile) $\beta_p = \mu_0 (R_0/a)^2 n_0 T_{e0}/B_0^2 = 0.01$, plasma current $I_P = 1.2$ MA, ohmic heating (no additional heating powers). The density profile were measured in 40 µs with a dwelt time 5 µs between two measurements. 5000 profiles were measured in 225 ms covering several sawtooth cycles. This peaking on axis has been shown to be due to the neoclassical Ware pinch and a drop of the particle diffusion [11]. The mexican hat like structure is not seen on the temperature which presents a smooth dome near the axis.

2.2 JET results

A very similar structure has been observed in JET ohmic shots as shown on Fig. 2. JET parameters are as follows : magnetic field on axis $B_0 = 2.55$ T, minor radius $a = 0.95$ m, major radius $R_0 = 2.9$ m, core density $n_0 = 3.0 \times 10^{19}$ m^{-3}, core electron temperature $T_{e0} = 1.8$ keV, plasma current $I_P = 2.25$ MA, ohmic heating (ICRH heating phase start at $t = 48$ s). The JET density profiles were reconstructed using the X-mode reflectometers [12]. JET reflectometers were swept simultaneously every 15 µs, this time covers the dwelt time between sweeps. 10000 profiles lasting 150 ms were recorded in the ohmic phase before ICRH heating phase.

2.3 2D tomography reconstruction

Using the mode rotation, 2-D reconstruction in a poloidal plane can be performed from 1-D radial profile. Such procedure was used for ECE temperature measurements [13]. On the Tore supra example, the density structures are observed using the reflectometry technique to rotate in the poloidal plane with a frequency F very close to 1 kHz, corresponding to an $m/n = 1/1$ internal kink mode, precursor or postcursor of the sawtooth. This frequency being much lower than the profile repetion rate $1/45$ µs, a tomographic inversion can be carried out [5]. The results are seen on Fig. 3. The sequence can be described as follows:

- A : after a crash, the density is almost flat inside the $q = 1$ surface and a peaking is seen to appear in the deepest core.
- B : a kink oscillation appears and the peaked core is displaced.
- C : The kink does not lead to a sawtooth crash but is later stabilized. Let us denote this a partial crash. The peak thus continues to grow.
- D : The peak is highest just before new kink oscillations appear in the core, this time leading to a sawtooth crash.
- E : After the sawtooth crash, a very distinct crescent-

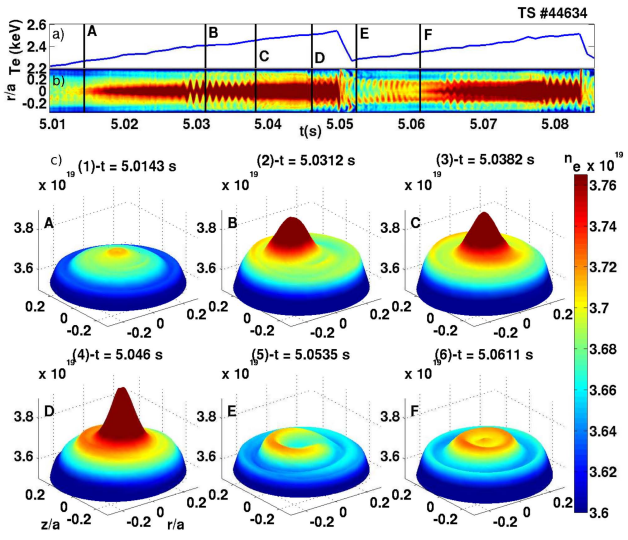

Fig. 3 Tore Supra pulse # 44634. Evolution of the central temperature (a), Time trace of the reflectometry signal (b) and tomographic reconstructions of the plasma electron density during a sawtooth (c). Vertical lines indicate the times at which snapshot are taken.

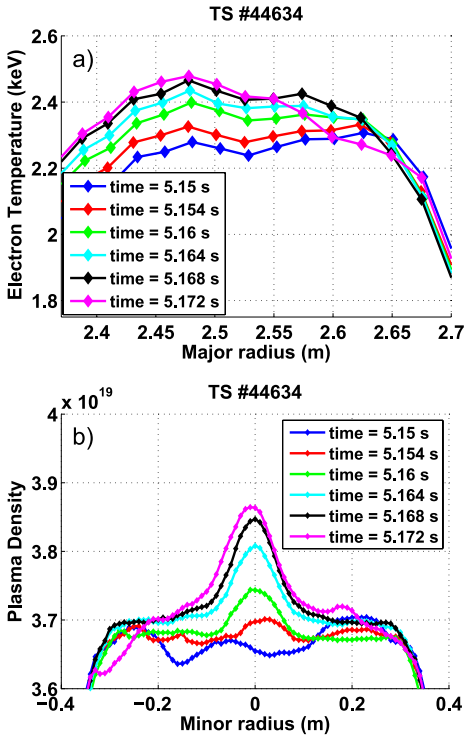

Fig. 4 Temperature profiles obtained by ECE measurements (a) and corresponding density profiles (b) during the ramp phase of the sawtooth. The magnetic axis ($r = 0$) is located at $R = 2.45$ m. Indicated times are in seconds.

shaped density structure can be observed inside the $q = 1$ surface. It formed during the reconnection phase because it is present immediately after the crash.

- F : After a few milliseconds, the crescent-shaped structure is seen to homogenize poloidally, while the peaking reappears in the center of the image. The main ring (orange) is encircled by a secondary ring (light blue).

Figure 4 displays the core density profiles together with the electron temperature measured using electron cyclotron emission, during the same pulse, but 150 ms later ($t = 5.15 - 5.17$ s). The peaking of the density profile is explained in part by a Ware pinch [11]. The experimental pinch velocity is of the order of $0.1\,\mathrm{m.s^{-1}}$ and can be considered as a constant for $r > 0.05$ m, where r is the minor radius. The overall sombrero shape of the profile, as observed on Fig. 4 b), can readily be explained. The divergence of the pinch flux $\nabla \cdot \left(n\boldsymbol{V}_{\mathrm{pinch}}\right)$ can be seen as a source term in the continuity equation, and for a constant radial velocity, there is an additional term in cylindrical geometry, compared to Cartesian geometry: $-n_{\mathrm{e}}|\boldsymbol{V}_{\mathrm{pinch}}|/r$, which enhances the effect of the pinch in the center. Hence, the evolution toward the equilibrium profile $\partial_{\mathrm{r}} n_{\mathrm{e}}/n_{\mathrm{e}} = |\boldsymbol{V}_{\mathrm{pinch}}|/D_{\perp}$, where $D_{\perp}$ is the transverse diffusion coefficient, is not homothetic and the profile looks more peaked in the center in the rise phase.

However, it is not sufficient to explain the observations. Closer examination of the blue, red and green profiles on Fig. 4 b) indicates strong flattening over a ring 0.2 m wide in only 10 ms. A diffusive process would require $D_{\perp} \simeq 4\,\mathrm{m^2.s^{-1}}$, while it was measured to be of the order of $0.05\,\mathrm{m^2.s^{-1}}$ in the deep core [11]. Also the flattening would most likely be seen on the temperature as well, but as shown on Fig. 4 a), the temperature profile does not exhibit such a flattening. Therefore, it is more likely explained by the MHD flows linked to the postcursor. Indeed the postcursor mode is present during the sequence blue → red → green, with same frequency and amplitude comparable to that of the precursor.

In the following, this flattening as well as the other structures observed on Fig. 3 are studied theoretically and numerically.

3. Numerical Methods

3.1 XTOR-2F

The XTOR-2F code is a nonlinear and bi-fluid full MHD code. It uses a fully-implicit scheme to solve the following set of equations [6] (assuming $p_{\mathrm{i}} = p_{\mathrm{e}} = p/2$):

$$\partial_{\mathrm{t}} n + \boldsymbol{v}\cdot\nabla n + n\nabla\cdot\boldsymbol{v} + \frac{\nabla p}{2e}\cdot\nabla\times\frac{\boldsymbol{B}}{B^2} = S_n + \nabla\cdot\left(D_{\perp}\nabla n - n\boldsymbol{V}_{\mathrm{pinch}}\right), \quad (1)$$

$$nm_{\mathrm{i}}\left(\partial_{\mathrm{t}}\boldsymbol{v} + \boldsymbol{v}\cdot\nabla\boldsymbol{v} + \boldsymbol{v}_{\mathrm{i}}^{\star}\cdot\nabla\boldsymbol{v}_{\perp}\right) - \boldsymbol{J}\times\boldsymbol{B} + \nabla p = \nu\nabla_{\perp}^2(\boldsymbol{v} + \boldsymbol{v}_{\mathrm{i}}^{\star}), \quad (2)$$

$$\partial_{\mathrm{t}} p + \boldsymbol{v}\cdot\nabla p + \Gamma p\nabla\cdot\boldsymbol{v} + \Gamma\frac{p}{2en}\nabla p\cdot\nabla\times\frac{\boldsymbol{B}}{B^2} = \chi_{\perp}\nabla_{\perp}^2 p + \nabla\cdot\left[\boldsymbol{B}\left(\frac{\rho\chi_{\parallel}}{B^2}\boldsymbol{B}\cdot\nabla\frac{p}{\rho}\right)\right] + S_{\mathrm{H}}, \quad (3)$$

$$\partial_t \boldsymbol{B} = \nabla \times (\boldsymbol{v} \times \boldsymbol{B}) + \nabla \times \frac{\nabla_{\parallel} p_e}{en} - \nabla \times \eta \boldsymbol{J}. \quad (4)$$

Here $\boldsymbol{v} = (\boldsymbol{E} \times \boldsymbol{B})/B^2 + \boldsymbol{v}_{\parallel i}$, $\boldsymbol{v}_i^{\star} = 1/(neB^2)\boldsymbol{B} \times \nabla p_i$ designates the ion diamagnetic velocity, $\perp$ and $\parallel$ refer to directions perpendicular and parallel to the magnetic field, i and e to ion and electron populations, S_n is a particle source that is vanishing in the core, S_H is a heating source, Γ is the ratio of specific heats, η the resistivity and $n = n_i = n_e$ (quasi-neutrality). The resistivity is tuned by the Lundquist number $S = \tau_R/\tau_A$, where $\tau_R = \mu_0 a^2/\eta$ is the resistive time and $\tau_A = (\mu_0 n_0 m_i)^{1/2} R_0/B_0$ is the Alfvén time. In the experiment, $S_{TS} = 2 \times 10^8$, while in XTOR-2F, $S \gg 10^7$ leads to prohibitive simulation times. Here, $S = 10^7$ is used.

3.2 Advection-diffusion 2D code

Even if XTOR-2F can produce kink instability leading to sawtooth collapse, it has not been found to exhibit the same fast flattening behaviour observed on Fig. 4 b). Indeed, reconnection is usually complete in XTOR-2F, so there is no free energy remaining for a postcursor mode, whereas a postcursor mode is usually observed in the experiment. However the flattening can be explained using what is known about the kink flow, without complex 3D nonlinear simulations. A simple bidimensional advection diffusion code has been written, solving for the density under the influence of a fixed potential velocity $\boldsymbol{v} = \hat{z} \times \nabla\phi$ and diffusion:

$$\partial_t n + (\hat{z} \times \nabla\phi) \cdot \nabla n = D_{\perp} \nabla_{\perp}^2 n. \quad (5)$$

The results are presented in the next section.

4. Analysis of Numerical Results

The flow linked with kink-type instability has been known for many years (see for example Ref. [14] for an extensive study of the kink structure). In the poloidal plane, the electric potential ϕ, which is the stream function, has typically the shape of two D-shaped vortices. However this holds only if there is no rotation of the mode in the poloidal plane, indeed in the rotating case, the electric potential is not the stream function anymore, since a stream function Φ must theoretically have the property $\partial_t \Phi = 0$, while here $\partial_t \phi \propto \omega\phi$. Hence we have to move to the frame rotating at the frequency of the perturbation, which adds a Doppler contribution to the potential: $\phi(r,\theta,t) \rightarrow \tilde{\phi}(r,\theta,t) = \phi(r,\theta-\omega t,t) - \phi_0$, where $\phi_0 = -1/2\omega B r^2$ [15]. Instead of two D-shaped vortices, Fig. 5 a), the potential now looks like the perturbed magnetic flux surfaces, as seen on Fig. 5 b). It is seen that the flow is significantly accelerated next to the $q = 1$ surface. Thus we propose the following flattening mechanism: starting after the sawtooth collapse with density gradients, the density is driven in the thin region close to the resonant surface where acceleration leads to the formation of filaments, rapidly smoothed by even a small diffusion.

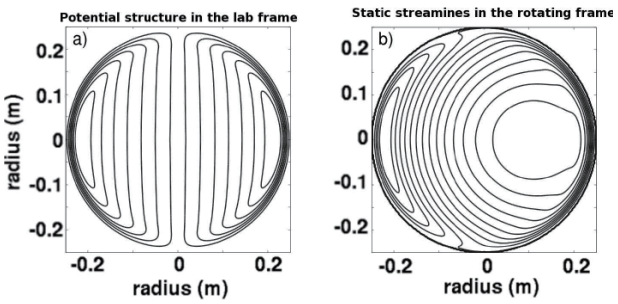

Fig. 5 Potential structure in the lab frame, obtained with XTOR-2F in the single fluid case (a) and corresponding stationary streamlines in the rotating frame (b).

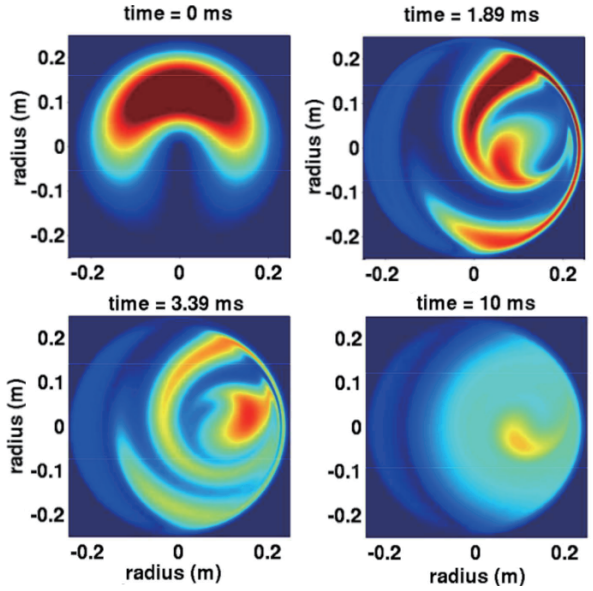

Fig. 6 The streamlines in Fig. 5 are used for an advection diffusion simulation with $r_s = 0.25\,\mathrm{m}$, $D = 0.05\,\mathrm{m}^2.\mathrm{s}^{-1}$, $f = 400\,\mathrm{Hz}$, $\xi_r(r=0) = 0.1\,\mathrm{m}$. Homogenization occurs in less than 10 ms.

We checked this mechanism with the advection code, using a postcursor amplitude and frequency, and an initial profile consistent with the experiment. The results are presented on Fig. 6, it is seen that indeed, flattening occurs very rapidly, in less than 10 ms.

Figure 7 displays the result of an XTOR-2F sawtooth crash simulation. The similarity of Fig. 7 with Fig. 3 is striking. In particular, the crescent-shaped structure observed in the experiment is recovered in the simulation (frame D'). As in the experiment, the crescent is encircled by a secondary ring (light blue on frames E and F of Fig. 3). The secondary ring represents the density which crossed the X-point during the reconnection process, and was mapped around the separatrix.

In more details, the sequence can be detailed as follows:

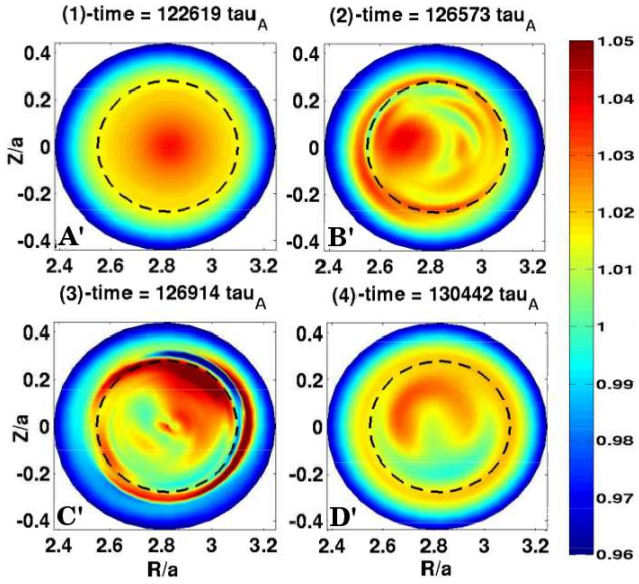

Fig. 7 Colour plots of the density in an XTOR-2F sawtooth crash simulation. The crescent-shaped structure is recovered and forms during the crash. Mode rotation is counter-clockwise. The dotted black circle figures the position of the initial $q = 1$ surface. It should not be confused with the separatrix which moves outward during reconnection.

- A': The peaked density is displayed prior to the kink destabilization.
- B': The dense core is driven toward the separatrix. Density starts crossing the X-point and is seen as a filament of density outside the $q = 1$ surface. First stages of reconnection are Kadomtsev-like.
- C': Reconnection accelerates because of diamagnetic effects.
- D': Reconnection stopped before all the particles crossed the separatrix. The dominant structure inside the $q = 1$ surface is crescent-shaped. The external structure homogenizes to form a ring outside the initial $q = 1$ surface.

The dominant term in the continuity equation during the reconnection process is the advection by the fast flows developed at the reconnection layer. The flow enters through the X-point (located on the top right region on frame C') and is accelerated to velocities of the order of the reduced poloidal Alfvén velocity $V^{\star}_{\mathrm{A}\theta} \equiv B_\theta(1-q)/\sqrt{\mu_0\rho} \simeq 0.01 V_\mathrm{A}$, where V_A is the Alfvén velocity, $V_\mathrm{A} \equiv B/\sqrt{\mu_0\rho}$. The process stops before all the particles contained inside the initial $q = 1$ surface have crossed the separatrix. This is obviously an evidence of break-down of the frozen-in-law. Indeed reconnection is complete, so all the helical flux inside the $q = 1$ surface is reconnected at the X-point, contrary to the particles. This discrepancy with the frozen-in-law comes from all the non-ideal processes allowed in XTOR-2F in Ohm's law, namely resistivity and bifluid effects, here the $\nabla \times (\nabla_\parallel p_\mathrm{e}/en)$ in *Eq.* (4). The latter term probably is the more crucial, since the aforementioned acceleration of the reconnection was attributed to this term being dominant over the resistivity (see [16]), and because poloidal pressure gradients are responsible for radial diamagnetic velocities, which change the magnetic field radial advection velocity compared to the particles advection velocity.

To explain the final crescent shape of the structure, let us note that after the crash, the safety factor is close to 1 everywhere inside the separatrix. There is no MHD activity remaining and the dominant homogenization process for the density is sound waves propagation linked with parallel gradients along the magnetic field. Such gradients are proportional to $m/n - q$, where m and n are the poloidal and toroidal wave numbers of the structure. Thus only mode numbers such that $m/n - q$ is very small are slowly damped, that is, only 1/1, 2/2, 3/3 and so on remain on long time scales. Eventually, the crescent-shaped structure homogenizes poloidally because q is not rigorously equal to 1, but in our simulation, this does not happen before the next crash occurs.

In the experiment, contrary to the XTOR-2F simulation, the different time scales: sawtooth period and post-crash profile relaxation time are distinct enough so that it is meaningful to compare the density content of the $q = 1$ surface before and after the sawtooth crash. Precisely, we compare the quantity $N_\mathrm{p}(t) = \oint\!\!\int_0^{r_\mathrm{inv}} (n_\mathrm{s}(\boldsymbol{r},t) - n_\mathrm{s}(r_\mathrm{inv},t_0))\,\mathrm{d}^3\boldsymbol{r}$ at two times t_0 and t_1 before and after the crash, which defines the reinjection ratio $f_\mathrm{p} = N_\mathrm{p}(t_1)/N_\mathrm{p}(t_0)$. Here r_inv is the inversion radius of the sawtooth. The quantity N_p is determined with one poloidal reconstruction assuming helical $m/n = 1/1$ symmetry. A flat profile inside the $q = 1$ surface would mean $f_\mathrm{p} = 0$. However, in the experiment, because of the crescent-shaped structure, this quantity is found to be of the order of 0.3 (± 0.2) in the 5 consecutive tomographically reconstructed sawtooth crashes. This means that a significant part of the density in excess of $n(r_\mathrm{inv})$ are not evacuated from the core, but stay inside, or, as suggested by the XTOR-2F simulations, are reinjected inside before the external density ring is flattened by diffusion.

This experimental result may have strong implications regarding impurity transport. Indeed in first approximation, the density of impurities can be considered as a passive scalar evolving in the plasma velocity field (but with their own diffusion coefficient). Since the density appears to be completely governed by the flows, it is likely that impurities would exhibit the same behaviour as the electron density. Thus our results imply that the sawtooth "flushing" mechanism to evacuate impurities such as fusion α-particles or high-Z impurities could be much less efficient than previously foreseen. XTOR-2F simulations taking impurities into account will be shortly undertaken.

5. Conclusion

Recent experimental results obtained with a novel fast-sweeping X-mode reflectometry technique give access to fine density structures in ohmic plasmas. These structures are tightly linked to the sawtooth dynamics. A significant density flattening has been shown to be consistent with the characteristics of the kink observed during postcursor oscillations.

The density is found to be redistributed inside the poloidal plane, with a reinjection ratio of the order of 0.3. After the crash, it is characterized by very specific ring and crescent-shaped structures. The XTOR-2F non-linear and bifluid full MHD code recovers the observed structures and helps understanding their dynamics. The $\boldsymbol{E} \times \boldsymbol{B}$ flows generated at the reconnection layer play the dominant role in the mechanism of their formation. These results have important implications regarding impurity transport.

The authors would like to thank F. Halpern and Z. Guimaraes for fruitful discussions. This work, supported by the European Communities under the contract of Association between EURATOM and CEA, was carried out within the framework of the European Fusion Development Agreement. The views and opinions expressed herein do not necessarily reflect those of the European Commission.

[1] R. Hastie, Astrophys. Space Sci. **256**(1-2), 177 (1998).
[2] F. Porcelli *et al.*, Plasma Phys. Control. Fusion **38**(12), 2163 (1996).
[3] J. Bucalossi *et al.*, In *39th EPS Conf. on Plasma Phys.* (2012).
[4] R. Sabot *et al.*, Nucl. Fusion **46**(9), S685. 7th International Reflectometry Workshop for Fusion Plasma Diagnostics (IRW7), Max Plank Inst Plasmaphys, Garching, GERMANY, MAY 09-12, 2005 (2006).
[5] R. Sabot *et al.*, In *37th EPS Conf. on Plasma Phys., Dublin (Ireland)* (2010).
[6] H. Lütjens *et al.*, J. Comput. Phys. **229**(21), 8130 (2010).
[7] C. Laviron *et al.*, Plasma Phys. Control. Fusion **38**(7), 905 (1996).
[8] P. Moreau *et al.*, Rev. Sci. Instrum. **71**(1), 74 (2000).
[9] R. Sabot *et al.*, Int. J. Infrared Milli. **25**(2), 229. 11th International Symposium on Laser-Aided Plasma Diagnotics, Houches, FRANCE, SEP 29-OCT 02, 2003 (2004).
[10] C. Gil *et al.*, Fusion Sci. Technol. **56**(3), 1219 (2009).
[11] R. Guirlet *et al.*, Nucl. Fusion **50**(9), 095009 (2010).
[12] A. Sirinelli *et al.*, Rev. Sci. Instrum. **81**(10), 10D939 (2010).
[13] Y. Nagayama *et al.*, Rev. Sci. Instrum. **61**(10, Part 2), 3265 (1990).
[14] H. Deblank *et al.*, Phys. Fluids B-Plasma **3**(5), 1136 (1991).
[15] T. Nicolas *et al.*, Phys. Plasmas **19**(11), 112305 (2012).
[16] F. Halpern *et al.*, Phys. Plasmas **18**(10), 102501 (2011).